# Directed ratchet transport in starlike networks of driven damped pendula by localized symmetry-breaking-inducing excitations

[1]R. Chacón, [2]A. Martínez García-Hoz, [3]P. J. Martínez, and [1]D. Durán
[1]*Departamento de Física Aplicada, E.I.I., Universidad de Extremadura, Apartado Postal 382, E-06006 Badajoz, Spain and Instituto de Computación Científica Avanzada (ICCAEx), Universidad de Extremadura, E-06006 Badajoz, Spain*
[2]*Departamento de Física Aplicada, E. T. S. de Ingenieros Agrónomos, Universidad de Castilla-La Mancha, E-13071 Ciudad Real, Spain and*
[3]*Departamento de Física Aplicada, E.I.N.A., Universidad de Zaragoza, E-50018 Zaragoza, Spain and Instituto de Nanociencia y Materiales de Aragón (INMA), CSIC-Universidad de Zaragoza, E-50009 Zaragoza, Spain*
(Dated: February 12, 2025)

We study the effectiveness of locally controlling the breakage of a significant space-time symmetry by zero-average periodic excitations at inducing and suppressing directed ratchet transport (i.e., that induced without an applied net bias) and chaos in starlike networks of driven damped pendula. While the emergence of chaos mainly depends upon the impulse transmitted by the periodic excitations, directed ratchet transport does upon a subtle balance between energy transmitted through the pendula via excitations' impulse and degree of symmetry breaking, thus defining a *physical criticality scenario*. Optimal enhancement of directed ratchet transport is found to occur when the waveform of the periodic excitation matches as closely as possible to an universal waveform when all nodes are homogeneously driven. In the case of networks with heterogeneous distributions of the symmetry breaking, the net ratcheting effect of increasing the effective breakage by periodic excitations acting on a number of particular nodes strongly depends upon their number and degree of connectivity as well as the coupling strength, while showing self-organized criticality with respect to the maximum strength of directed ratchet transport.

## I. INTRODUCTION

Exploring directed ratchet transport (DRT) phenomena in complex networks is currently a fundamental task for the nonlinear science community since the interactions among single-particle ratchets cannot be neglected in general−molecular motors being a paradigmatic example. Of particular importance is the goal of controlling the strength and direction of DRT in complex networks [1-5] of inertial ratchets which are capable of exhibiting chaos when they are isolated [6]. Previous studies of coupled inertial ratchets include the possibility, under certain conditions, of coupling-induced enhancement of the average velocity [7], bifurcations, synchronization, and current reversals in two coupled sinusoidally driven ratchets [8,9], DRT of topological solitons in damped, biharmonically driven Frenkel-Kontorova chains [10] as well as synchronization phenomena and transport properties of inertial particles in networks subjected to random long-range interactions [11,12].

While most previous studies of coupled inertial ratchets subjected to periodic excitations have mainly focused on local (homogeneous) diffusive-type coupling, very few have explored the possible influences of the existence of heterogeneous connectivity on transport properties of a network of chaotic nodes. Heterogeneous connectivity in the form of a scale-free topology [13] is a common property of many different biological and technological real-world networks. It means that just a small set of nodes −so-called hubs− are highly connected while the rest of the nodes have few connections. Since starlike structures are the main motifs of scale-free networks, we here investigate the control of DRT and associated chaotic and synchronization phenomena in starlike networks (SNs) of dissipative nonlinear oscillators by locally controlling the breakage of a generalized parity symmetry [cf. Eq. (3)] by zero-average periodic excitations. Thus, a major motivation for the present study was we expected that the main characteristics of such a DRT scenario could well be extensible to the case of scale-free networks. Also, chaos control and synchronization are closely related phenomena [14,15], and there have been studies published of diverse synchronization phenomena in oscillator networks with starlike couplings [16-20].

On the other hand, the theory of *ratchet universality* (RU) [21-23] provides a subtle law of nature that establishes the existence of a universal (magic) force waveform which optimally enhances directed transport by symmetry breaking. This law comes from a physical scenario of criticality that emerges when the generalized parity symmetry and the generalized time-reversal symmetry are broken, regardless of the nature of the dynamic equation in which the breaking of such symmetries results in DRT. The law of RU has been confirmed in quite varied physical contexts in which the driving forces are chosen to be biharmonic, such as in the instances of topological solitons [10], Bose-Einstein condensates exposed to a sawtooth-like optical lattice potential [24], matter-wave solitons [25], one-dimensional granular chains [26], and Bose-Einstein condensates under an unbiased periodic driving potential [27]. Also, the efficiency of RU in quantum systems has been previously shown, including the examples of directed transport of atoms in a Hamil-

tonian quantum ratchet [24] and driven Bose-Einstein condensates [27]. Remarkably, the law of RU has also explained the interplay between symmetry breaking and thermal noise in the DRT of a Brownian particle moving on a periodic substrate subjected to a homogeneous temporal biharmonic force [28-30], and the DRT scenario of a driven Brownian particle subjected to a vibrating periodic potential [31]. Numerical studies of a driven Brownian particle in the presence of non-Gaussian noise [32] and coupled Brownian motors with random interactions in a congested environment [33] have supported the RU predictions. Furthermore, RU has been demonstrated in the bidirectional escape from a symmetric potential well [34], coupled dissipative oscillators in the absence of external bias [35], experimental DRT of fluxons and cold atoms driven by biharmonic fields [36] as well as in the DRT of spheres in viscous fluids [37]. Lately, analytical and numerical studies of DRT of a particle on a horizontal surface under biharmonic vibrations have supported the RU predictions [38].

The present work discusses a topology-induced DRT scenario in SNs of dissipative non-autonomous systems subjected to local transport-inducing periodic excitations while keeping their common amplitude and period fixed. Specifically, the results will be discussed through the analysis of SNs of $N$ driven damped pendula—see Fig. 1(a). The driven damped pendulum is a paradigmatic model allowing analytical exploration while exhibiting universal characteristics which are representative of many dissipative real-world systems. The complete model system reads

$$\ddot{x}_H + \sin x_H = -\delta \dot{x}_H + \gamma f_H(t) + \lambda \sum_{i=1}^{N-1} \sin\left(x_i - x_H\right),$$
$$\ddot{x}_i + \sin x_i = -\delta \dot{x}_i + \gamma f_i(t) + \lambda \sin\left(x_H - x_i\right), \qquad (1)$$

$i = 1, ..., N-1$, where $f_{H,i}(t)$ is a zero-mean unit-amplitude $T$-periodic excitation:

$$f_{H,i}(t) = 2\,\mathrm{sn}\left(\Omega_{H,i} t; m_{H,i}\right) \mathrm{cn}\left(\Omega_{H,i} t; m_{H,i}\right), \qquad (2)$$

where all variables and parameters are dimensionless: $\Omega_{H,i} = \Omega_{H,i}\left(T, m_{H,i}\right) \equiv 2K(m_{H,i})/T$, $T$ and $\gamma$ are the common excitation period and amplitude, respectively, $\delta$ is the damping coefficient, $\lambda$ is the coupling constant, $\mathrm{sn}\left(\cdot; m\right), \mathrm{cn}\left(\cdot; m\right)$ are Jacobian elliptic functions of parameter $m$, $K(m)$ is the complete elliptic integral of the first kind, while the elliptic periodic excitation $f_{H,i}(t)$ has the same amplitude 1 and period $T$ for any waveform (i.e., $\forall m \in [0, 1[$, see Fig. 1 (b)). Notice that the coupling constant does not scale with $N$, unlike other model systems such as the Kuramoto model. Equations (1) describe the dynamics of a highly connected pendulum (or hub), $x_H$, and $N-1$ linked pendula (or leaves), $x_i$. When the periodic excitation presents the shift symmetry $[f_{H,i}(t + T/2) = -f_{H,i}(t)]$, the system Eq. (1) presents the generalized parity symmetry

$$\mathbf{S} : x_{H,i} \to -x_{H,i},\ t \to t + T/2, \qquad (3)$$

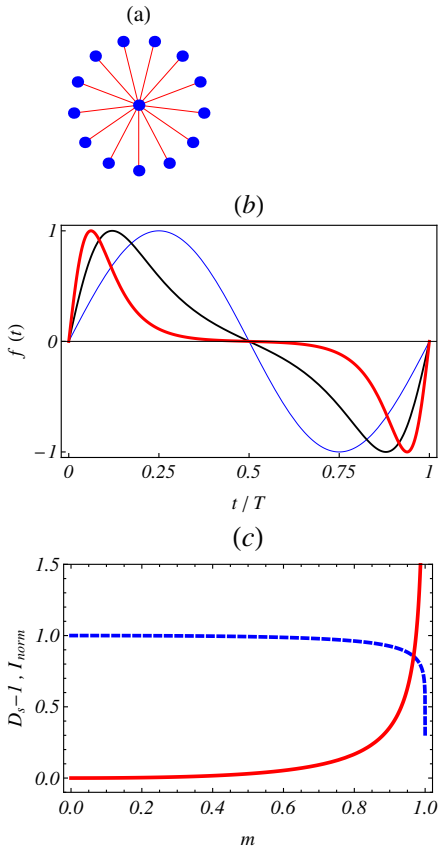


FIG. 1: (a) Schematic representation of a starlike network of $N = 14$ pendula. (b) Elliptic function $f_{ellip}(t) \equiv 2\,\mathrm{sn}\left[2K(m)t/T; m\right]\mathrm{cn}\left[2K(m)t/T; m\right]$ [cf. Eq. (2)] vs $t/T$ for $m = 0$ [thin (blue) line], $m = 0.989$ [medium (black) line], and $m = 0.99999$ [thick (red) line]. (c) Normalized impulse $I_{norm} \equiv I(m)/I(m = 0)$ [cf. Eq. (4); dashed line] and the quantifier of the degree of symmetry breaking associated with the periodic excitation shift symmetry [cf. Eq. (5)] vs the shape parameter $m$. The quantities plotted are dimensionless.

$i = 1, ..., N-1$, i.e., nonsymmetric stationary solutions always occur in pairs, and hence DRT is not possible. To explore the emergence of DRT in SN Eq. (1), the periodic excitation $f_{H,i}(t)$ was chosen to exhibit four remarkable properties. First, its waveform (and hence its impulse) is changed by solely varying a *single* parameter, the shape parameter $m$, between 0 and 1. Second, when $m = 0$ then $f_{H,i}(t) = \sin\left(2\pi t/T\right)$, i.e., one recovers the standard case of a harmonic periodic excitation [39,40], while, for the limiting value $m = 1$, $f_{H,i}(t)$ vanishes; i.e., DRT is not possible for these two limiting values, while it is expected for $0 < m < 1$. Third, the periodic excitation's impulse per unit of period,

$$I\left(m\right) \equiv \frac{1}{T}\int_0^{T/2} f_{H,i}(t)dt = \frac{1}{K(m)\left(1+\sqrt{1-m}\right)}, \qquad (4)$$

is a monotonously decreasing function of the shape pa-

rameter [see Fig. 1(c)]. And fourth, the quantifier of the degree of symmetry breaking [21] associated with the periodic excitation shift symmetry is a monotonously increasing function of the shape parameter:

$$D_s[f_{H,i}] \equiv \left\langle \frac{-f_{H,i}\left(t+T/2\right)}{f_{H,i}\left(t\right)} \right\rangle_T \equiv \frac{1}{T}\int_0^T \frac{-f_{H,i}\left(t+T/2\right)}{f_{H,i}\left(t\right)} dt = \frac{E(m)}{\sqrt{1-m}K(m)}, \tag{5}$$

where $E(m)$ is the complete elliptic integral of the second kind [41] [see Fig. 1(c)]. For SNs subjected to a *homogeneous* periodic excitation, this means that the strength of DRT is expected to present a maximum at a certain critical value $m = m_c$ as the shape parameter is varied, while keeping constant the remaining parameters of the SN. Furthermore, RU predicts $m_c$ to be near $m = 0.984$ since the optimal values of $a_1(m), a_2(m)$ for the biharmonic approximation of the Fourier series

$$f_{H,i}(t) \equiv \sum_{n=1}^{\infty} a_n(m) \sin\left(\frac{2n\pi t}{T}\right), \quad a_n(m) \equiv \frac{2n\pi^2}{mK^2(m)} \operatorname{sech}\left[\frac{n\pi K(1-m)}{K(m)}\right], \tag{6}$$

are recovered at $m = 0.984$ (see Refs. [21,34] for additional details).

In the present work, we shall study the interplay between heterogeneous connectivity and localized symmetry-breaking-induced *emergence and control* of DRT for $\lambda > 0, m_{H,i} \geqslant 0$, i.e., the shape parameter is taken to be $m = 0$ except for certain sets of pendula that are subjected to periodic excitations of variable waveform ($m \in ]0, 1[$). In particular, we shall provide a generic answer to the question of where the energy needed for DRT comes from.

The remainder of the article is structured as follows. Section II investigates the chaotic behavior of isolated pendula [Eq.(1) with $\lambda = 0$]. We compare the analytical estimates of the chaotic threshold in parameter space obtained by using Melnikov's method (MM) [42,43] with those using Lyapunov exponent (LE) calculations [44]. The interplay between heterogeneous connectivity and local breaking (increase and decrease) of the periodic excitation's shift symmetry in networks described by Eq. (1) is studied in Sec. III. We characterize a fairly complex DRT scenario including the role of chaos, and determine how the effectiveness of local symmetry-breaking periodic excitations at controlling DRT depends not only upon the coupling strength but also on the number of control nodes and their degree of connectivity. Finally, we summarize the findings and discuss some open problems in Sec. IV.

## II. ISOLATED PENDULUM

Before discussing the chaos and DRT scenarios of driven damped pendula coupled in a starlike topology, it is essential to understand the main characteristics of the dynamics of an isolated driven damped pendulum:

$$\ddot{x} + \sin x = -\delta\dot{x} + \gamma f_{ellip}(t), \tag{7}$$

where

$$f_{ellip}(t) \equiv 2\,\mathrm{sn}\left[2K\left(m\right)t/T; m\right]\mathrm{cn}\left[2K\left(m\right)t/T; m\right] \tag{8}$$

is the elliptic periodic excitation [cf. Eq. (2)]. In particular, we are interested in comparing analytical and numerical estimates of the order-chaos threshold in parameter space, providing theoretical arguments showing that the equilibrium $\left(x = 0, \dot{x} = 0\right)$ may be a stable attractor of Eq. (7) for periodic excitations of a certain waveform ($m < 1$) as well as the possibility of impulse-induced suppression of chaos. The following two subsections are dedicated to describing these analyses separately.

### A. Chaotic threshold

To obtain analytical estimates of the chaotic threshold in parameter space $(\gamma, \delta, T, m)$, we assume that the driven damped pendulum (7) satisfies the MM requirements, i.e., the dissipation and periodic excitation terms are small-amplitude perturbations of the underlying conservative pendulum $\ddot{x} + \sin x = 0$. As is well-known, the so-called Melnikov function, $M\left(t_0\right)$, provides a measure of the distance between the perturbed stable and unstable manifolds in the Poincaré section at $t_0$. If the Melnikov function presents a simple zero, the manifolds intersect transversally and chaotic instabilities result (see, e.g., Refs. [42,43] for further details about MM). Thus, after using the Fourier series of the elliptic periodic excitation $f_{ellip}(t)$ [cf. Eq. (6)] [45], the application of MM to Eq. (7) yields the Melnikov function

$$M^{\pm}\left(t_0\right) = -D \mp \gamma \sum_{n=1}^{\infty} a_n\left(m\right) b_n\left(T\right) \sin\left(\frac{2n\pi t_0}{T}\right), \quad D \equiv 8\delta, \quad a_n\left(m\right) \equiv \frac{2n\pi^2}{mK^2(m)} \operatorname{sech}\left[\frac{n\pi K(1-m)}{K(m)}\right], \quad b_n\left(T\right) \equiv 2\pi \operatorname{sech}\left(\frac{n\pi^2}{T}\right), \tag{9}$$

where the positive (negative) sign refers to the top (bottom) homoclinic orbit of the underlying conservative pendulum: $x_0\left(t\right) = \pm 2\arctan\left[\sinh\left(t\right)\right]$, $\dot{x}_0\left(t\right) = \pm 2\operatorname{sech}\left(t\right)$. If $M^{\pm}\left(t_0\right)$ has a simple zero, then a heteroclinic bifurcation occurs, signifying the onset of chaotic instabilities. From Eq. (9) one sees that an upper bound can

be obtained in closed form for each pair of harmonics of frequencies $\omega_n \equiv 2n\pi/T$ and $2\omega_n$, and hence

$$\begin{aligned}&\sum_{n=1}^{\infty} a_n(m)\, b_n(T) \sin\left(\frac{2n\pi t_0}{T}\right)\\ &\leqslant \sum_{n=1}^{\infty} a_n(m)\, b_n(T) \sin(\omega_n t_{0n}^*)\\ &+ \sum_{n=1}^{\infty} a_{2n}(m)\, b_{2n}(T) \sin(2\omega_n t_{0n}^*)\,, \end{aligned} \tag{10}$$

where

$$t_{0n}^* \equiv \omega_n^{-1} \arccos\left\{ \frac{\sqrt{1+32\left[\frac{a_{2n}(m) b_{2n}(T)}{a_n(m) b_n(T)}\right]^2}-1}{8 a_{2n}(m)\, b_{2n}(T) / [a_n(m)\, b_n(T)]} \right\}. \tag{11}$$

It is worth noting that the upper bound given by Eq. (10) is less than the straightforward bound given by $\sum_{n=1}^{\infty} a_n(m)\, b_n(T)$. If the damping coefficient is such that

$$\begin{aligned} D &\geqslant \gamma \sum_{n=1}^{\infty} c_n(m,T)\,,\\ c_n(m,T) &\equiv a_n(m)\, b_n(T) \sin(\omega_n t_{0n}^*)\\ &\quad + a_{2n}(m)\, b_{2n}(T) \sin(2\omega_n t_{0n}^*)\,, \end{aligned} \tag{12}$$

this relationship represents a sufficient condition for $M^{\pm}(t_0)$ to always have the same sign, i.e., $M^{\pm}(t_0) \leqslant 0$. Thus, a *necessary* condition for $M^{\pm}(t_0)$ to change sign at some $t_0$ is written

$$\frac{\delta}{\gamma} < U_{th}(T,m)\,, \tag{13}$$

where the chaotic threshold function scales as

$$U_{th}(T,m) \sim \frac{1}{8} \sum_{n=1}^{\infty} c_n(m,T)\,. \tag{14}$$

From Eq. (14) one readily obtains

$$\lim_{T\to 0} U_{th}(T,m) = \lim_{m\to 1} U_{th}(T,m) = 0, \tag{15}$$

i.e., in such limits chaotic dynamics is not expected. A plot of $U_{th}(T,m)$ is shown in Fig. 2 top. Let us consider the chaotic threshold function as a function of $T$, holding $m$ constant. Plots of $U_{th}(T, m = const)$ show each curve to present a monotonously increasing behavior for any value of the shape parameter $m$ (cf. Fig. 2 middle). Now we study the chaotic threshold function as a function of $m$, holding $T$ constant. Plots of $U_{th}(T = const, m)$ show each curve to present a maximum $m_{\max} = m_{\max}(T)$ from a certain critical period $T > T_c \approx 6$, while a monotonously decreasing behavior is found for $T \leqslant T_c$ (cf. Fig. 2 bottom). Thus, these MM-based predictions

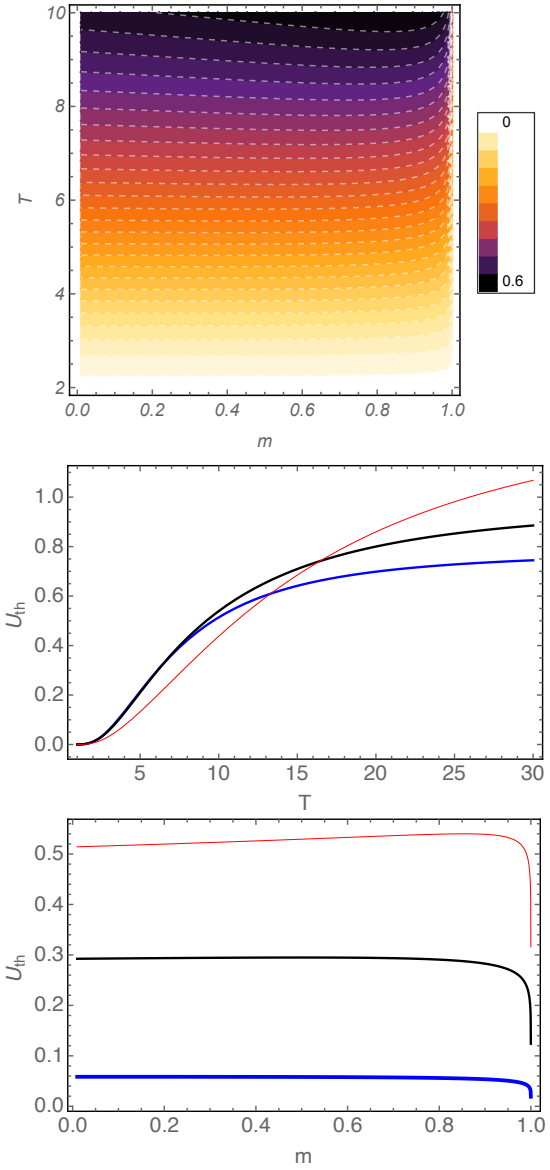


FIG. 2: Top: Contour plot of the chaotic threshold function $U_{th} \equiv U_{th}(T,m)$ [cf. Eq. (14)] vs shape parameter $m$ and period $T$ for an isolated pendulum ($\lambda = 0$). Middle: Chaotic threshold function $U_{th}$ [cf. Eq. (14)] vs period $T$ for $m = 0$ [thick (blue) line], $m = 0.8$ [medium (black) line], and $m = 0.999$ [thin (red) line]. Bottom: Chaotic threshold function $U_{th}$ [cf. Eq. (14)] vs $m$ for $T = 3$ [thick (blue) line], $T = 6$ [medium (black) line], and $T = 10$ [thin (red) line]. The quantities plotted are dimensionless.

indicate that carefully fitting the waveform of the periodic excitation, in particular when $T > T_c$, is a reliable procedure for inducing chaos while keeping the remaining parameters constant.

Next, we shall compare the chaotic threshold predicted from MM and LE calculations. One cannot expect too good a quantitative agreement between the two types of results because MM is generally related with transient chaos while LE provides information concerning only

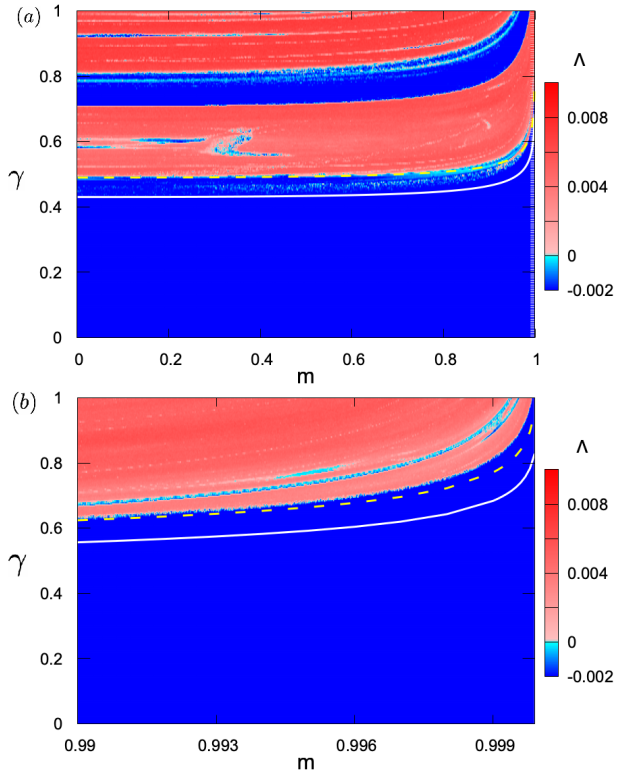


FIG. 3: (a) Distribution of the maximal Lyapunov exponent in the $m-\gamma$ parameter plane for an isolated pendulum ($\lambda = 0$) and $T = 9.4, \delta = 0.1$. The dashed and solid lines denote the theoretical estimate of the chaotic boundary $\gamma = \gamma_{th} = 2.4\times\delta/U_{th}\,(T = 9.4, m)$ [cf. Eq. (14)] from Melnikov's method and an inverse-impulse fitting $\gamma_c = 12.9\times\delta/I(m)$ [cf. Eqs. (4) and (20)], respectively. (b) Magnification of version (a) corresponding to the range $m \in [0.99, 1]$. The quantities plotted are dimensionless.

steady motions, i.e., a positive maximal LE always indicates the presence of a chaotic strange attractor (steady chaos) while a chaotic transient does not necessarily lead to one of such chaotic attractors. We compute the LEs by using a version of the algorithm discussed in Ref. [44]. We typically integrate up to $10^4$ drive cycles for fixed values of the parameters $T, \delta$ and calculate the maximal LE for each point on a $120 \times 120$ grid in the $m - \gamma$ parameter plane. Figure 3 shows an illustrative instance for the values $T = 9.4 > T_c, \delta = 0.1$. The chaotic threshold (solid line in Fig. 3) predicted from MM provides a qualitative estimate for the lower boundary of the entire chaotic region, as expected (recall the abovementioned caveats). Nevertheless, the theoretical estimate captures a main characteristic of the numerically-obtained chaotic boundary, namely, it presents monotonously increasing behaviour as a function of the shape parameter from $m \approx m_{\max}\,(T = 9.4)$. We will show in Sec. III how numerical simulations of SNs of driven damped pendula confirmed the usefulness of this chaos-control scenario when the pendula couple ($\lambda > 0$).

### B. Energy-based analysis

After analysing the variation of the pendulum's energy, one can predict the impulse-induced suppression of chaos via the phenomenon of amplitude death [46]. Indeed, Eq. (3) has the associated energy equation

$$\frac{dE}{dt} = -\delta\dot{x}^2 + \gamma f_{ellip}(t)\dot{x}, \tag{16}$$

where $E(t) \equiv (1/2)\,\dot{x}^2\,(t) - \cos[x\,(t)]$ is the energy function and $f_{ellip}(t)$ is the elliptic excitation [cf. Eq. (8)]. Integration of Eq. (16) over *any* interval $[nT, nT + T/2]$, $n = 0, 1, 2, ...$, yields

$$E\,(nT + T/2) = E(nT) - \delta\int_{nT}^{nT+T/2}\dot{x}^2\,(t)\,dt + \gamma\int_{nT}^{nT+T/2} f_{ellip}(t)\dot{x}\,(t)\,dt. \tag{17}$$

Now, after applying the first mean value theorem for integrals [47] together with well-known properties of the Jacobian elliptic functions [41] to the last two integrals on the right-hand side of Eq. (17), one has

$$E\,(nT + T/2) = E(nT) - \delta\dot{x}^2\,(t^{**})\,T/2 + \gamma\dot{x}\,(t^*)\,I\,(m)\,T, \tag{18}$$

where $t^*, t^{**} \in [nT, nT + T/2]$, and $I\,(m)$ is the impulse transmitted per unit of period [cf. Eq. (4); see Fig. 1(c)]. Next, we discuss the possibility of the phenomenon of amplitude death. By fixing the parameters $(\delta, \gamma, T)$ for the driven damped pendulum to exhibit chaotic dynamics at $m = m_{\max}\,(T)$, there always exists an $n = n^*$ such that the energy increment

$$\Delta E^{m=m_{\max}(T)} \equiv E\,(n^*T + T/2) - E(n^*T) > 0. \tag{19}$$

In this situation, one decreases the impulse by increasing the shape parameter from $m = m_{\max}\,(T)$ while holding the remaining parameters constant. Equations (18) and (19) predict that, for each $n^*$, there always exists a minimum critical value $m = m_c > m_{\max}\,(T)$ such that the corresponding energy increment $\Delta E^{m=m_c} < 0$ for *all* $n > n^*$, and hence the equilibrium $\left(x = 0, \dot{x} = 0\right)$ is the single attractor of the driven damped pendulum for $m \geqslant m_c$. Note that this property comes ultimately from the behaviour of the impulse $I\,(m)$ as the shape parameter $m \to 1$ [cf. Fig. 1(c)], i.e., that the driven damped pendulum effectively behaves as a purely damped pendulum for sufficiently narrow pulses. Thus, one straightforwardly obtains from Eqs. (18) and (19) that, for periodic excitations having sufficiently narrow pulses, the equilibrium $\left(x = 0, \dot{x} = 0\right)$ is the single attractor of the driven damped pendulum when $\gamma < \gamma_c$, where the critical amplitude scales as

$$\gamma_c \sim \delta/I(m). \tag{20}$$

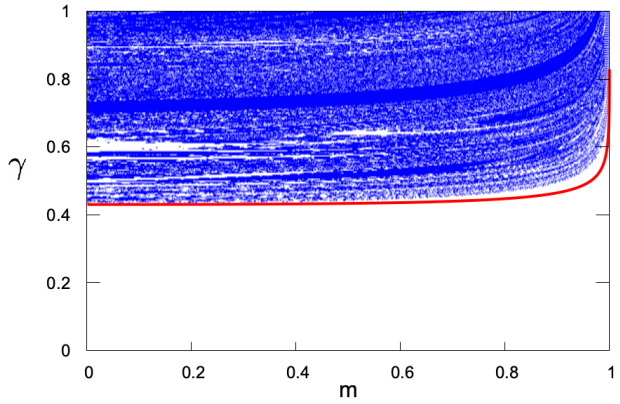


FIG. 4: Stability boundary of the equilibrium $(x = 0, \dot{x} = 0)$ in the $m-\gamma$ parameter plane for an isolated pendulum ($\lambda = 0$) and $T = 9.4, \delta = 0.1$. The instability region (dots) was calculated numerically on a grid of $1000 \times 200$ points. The solid line denotes the theoretical estimate of the stability boundary $\gamma_c = 12.9 \times \delta / I(m)$ from Eq. (20). The quantities plotted are dimensionless.

Our numerical simulations confirmed the validity of the scaling given by Eq. (20) for periodic excitations having sufficiently narrow pulses, as in the instance shown in Fig. 4.

## III. LOCALIZED CONTROL OF RATCHET TRANSPORT IN STARLIKE NETWORKS

In this section, we shall explore the relative effectiveness of locally controlling both the breakage of the generalized parity symmetry [Eq. (3)] and the emergence of chaos by periodic excitations [Eq. (2)], in the sense of varying their shape parameter $m$, on $M$ nodes of SNs of $N$ driven damped pendula [cf. Eq. (1), $M \leq N$] while keeping the remaining parameters constant. Equation (1) was numerically integrated using a fourth-order Runge-Kutta algorithm with time step $dt = T/100$. To describe the overall spatiotemporal dynamics of networks, we first calculated the average velocity

$$\sigma\left(jT\right) \equiv (1/N) \sum_{i=1}^{N} \frac{dx_i}{dt}\left(jT\right), \tag{21}$$

where $j$ is an integer multiple of the driving period $T$, and then calculate

$$V \equiv \langle \langle \sigma\left(jT\right) \rangle_t \rangle_{ic}, \tag{22}$$

where $\langle \cdot \rangle_t$ and $\langle \cdot \rangle_{ic}$ indicate time averaging over a established (sufficiently long) study window and averaging over a uniform and symmetric set of initial conditions within the initial potential well, respectively. The degree of synchronization is characterized by first calculating the correlation function [48]

$$Corr \equiv \frac{2}{N(N-1)} \sum_{(il)} \langle \cos\left(x_i - x_l\right) \rangle_t, \tag{23}$$

and then calculating its average over the aforementioned set of initial conditions

$$C \equiv \langle Corr \rangle_{ic}. \tag{24}$$

Observe that $Corr$ is 1 for the perfectly synchronized state, whereas desynchronization increases as $Corr$ decreases from 1. Before applying any control, we assume a set of fixed parameters $(\gamma, \delta, T)$ such that each isolated pendulum subjected to a sinusoidal periodic excitation ($m_H = m_i = 0, i = 1, ..., N-1$) displays chaotic behaviour, while the corresponding SN of such sinusoidally excited pendula displays chaotic behaviour too.

### A. Control of all pendula

Let us first consider the effect of controlling the breakage of the generalized parity symmetry [Eq. (3)] in the same way in all pendula of the SN, i.e., $m_H = m_i, i = 1, ..., N-1$. For suprathreshold amplitudes, we typically found an increase of the absolute value of the average velocity $|V|$ from $V = 0$ at $m = 0$ up to the absolute maximum $|V| = V_{\max}^{unif}$ at $m = m_{\max}^{unif} \approx 0.989$ followed by a decrease to $V = 0$ at $m = 1$ in both strong and weak coupling regimes, as in the instance shown in Fig. 5 in which the absolute maximum velocity corresponds to a synchronized periodic clockwise rotation. Notice that the overall decrease of $|V|$ from $m = m_{\max}^{unif}$ to $m = 1$ is a direct consequence of the behavior described above for isolated pendula (cf. Sec. II). The average velocity presents additional secondary extrema at different values of the shape parameter which are typically associated with complete synchronization states (compare Figs. 5 and 6). These extrema typically correspond to phase-locked rotation states of all or most of the pendula and appear over certain finite ranges of the shape parameter where $V \propto (p/q)\, T^{-1}$has a constant value, with $p$ and $q$ being coprime integers, while they satisfy the commensurability relationship $T_s/T = 1$ (main resonance), where $T_s$ is the period of the synchronized periodic rotation. For the case shown in Fig. 5, one has $V = 2\pi p T^{-1}$, $p = 4, 2, 3$ for the extrema roughly centered at the values $m = 0.9897, 0.9936, 0.9985$, respectively. Note that the slow increase of $|V|$ in the range of small values of the shape parameter resembles that of the quantifier $D_s$ [cf. Eq. (5)] in the same range (compare Figs. 5(a) and 1(c)), in accordance with the degree of symmetry breaking mechanism [21]. Also, Fig. 5 shows that *reshaping-induced* current reversals occur at certain values of the shape parameter $m$ as well as the possibility that there is no transport at all over certain ranges of the shape parameter (see Fig. 5(b)) because the only attractor of the SN is the equilibrium $\left(x_{H,i} = \dot{x}_{H,i} = 0, i = 1, ..., N-1\right)$ which, in turn, is due to the phenomenon of amplitude death (cf. Sec. II B). In order to clarify the mechanism giving rise to these current reversals, we calculated bifurcation diagrams of the average velocity $\sigma$ [cf. Eq. (21)]

and the maximal LE $\Lambda$ [see Figs. 5(d) and 5(e)]. Although Figs. 5(d) and 5(e) were obtained for a single, randomly chosen initial condition, comparison of these with Figs. 5(a) and 5(b), respectively, indicates a certain correlation between current reversals and chaos-order transitions. It is worth mentioning that this correlation has been previously reported in the context of a damped-driven particle subjected to a biharmonic ratchet potential [6]. Note, however, that not all chaos-order transitions are associated with current reversals, such as the one occurring just before the value $m = m_{\max}^{unif} \approx 0.989$ (compare Figs. 5(c) and 5(e)). As expected, the degree of synchronization increases with the coupling constant from the weak coupling regime, where desynchronization states typically appear due to cluster synchronization of different sets of pendula, to the strong coupling regime where the SN presents complete synchronization states (see Fig. 6).

### B. Control only of the central pendulum

An interesting question to investigate is the singular effect of solely breaking the periodic excitation's shift symmetry in the hub ($M = 1$), while the $N - 1$ leaves remain subjected to symmetric (i.e., sinusoidal: $m_i = 0$, $i = 1, ..., N - 1$) periodic excitations. The overall behavior of the average velocity $V$ as a function of the shape parameter $m$ is typically similar to that found in the case of homogeneous symmetry breaking in all pendula of the SN. Figure 7 shows instances of such behavior for networks in the strong coupling regime and increasing values of the SN size (compare Figs. 5 and 7).

We obtained that the $m$ value at which $|V|$ presents an absolute maximum, $m_{\max}(N)$, increases monotonously with the number of leaves, while the corresponding absolute (critical) value of the maximum average velocity, $V_{\max} \equiv V(m = m_{\max}(N))$, does not depend significantly on $N$, indicating thus self-organized criticality, as is shown in Fig. 8.

For sufficiently high values of the coupling constant $\lambda$, one systematically obtains $m_{\max}(N) \geq m_{\max}^{unif}$ from a relatively small value of the SN size and $m_{\max}(N) \leq m_{\max}^{unif}$ for the smallest SNs ($N \geq 4$ and $N = 2, 3$, respectively, in the instance shown in Fig. 8). Also, the value $V_{\max}^{unif}$ corresponding to the case of homogeneous symmetry breaking in all pendula is always higher than the value $V(m = m_{\max}(N))$ for any size of SN, as expected from the degree of symmetry breaking mechanism. Thus, optimal collective DRT requires a greater increase in the degree of symmetry breaking than in the case of homogeneous symmetry breaking in all pendula when the number of leaves is high enough, while the maximum strength of DRT is systematically higher in the homogeneous case than in the present heterogeneous case. This behavior can be understood taking into account that the average kinetic energy of each uncoupled pendula scale as

$$\left\langle \dot{x}_{H,i}^2 \right\rangle \sim \frac{\gamma}{\delta} I(m_{H,i}), \tag{25}$$

$i = 1, ..., N - 1$, where brackets indicate time average (see derivation in [23]). Although the symmetric periodic excitations acting on the leaves does not yield DRT, they inject energy into the leaves through the periodic excitation's impulse, which is transmitted to the hub via the bidirectional coupling. Since all pendula are identical, except for the impulse of their periodic excitations, this energy flow from the leaves to the hub increases the kinetic energy of the hub on average, thus favoring transport in it. But DRT only originates from the hub, which will need less symmetry breaking than in the homogeneous symmetry-breaking case to produce collective DRT if the number of leaves is sufficiently small (the hub has to command the motion of a few leaves with the aid of a slight increase in its average kinetic energy), while it will need more symmetry breaking to produce DRT in all pendula if the number of leaves is significantly large in the sense of the energy they inject into the hub (even with the aid of a significant increase in its average kinetic energy, the hub has to command the motion of many leaves). Notice that this physical self-organized criticality scenario for DRT in SNs strongly depends upon the coupling constant due to the needed balance between the energy transmitted through the pendula via excitations' impulse and the degree of symmetry breaking giving rise to DRT.

### C. Control only of peripheral pendula

Next, we explore the complementary case to that of the previous subsection, i.e., the accumulative effect of homogeneously breaking the periodic excitation's shift symmetry on all the leaves ($M = N - 1$), while the hub remains subjected to symmetric (i.e., sinusoidal: $m_H = 0$) periodic excitations. Similarly to the previous complementary case, we typically obtained an overall behavior of the average velocity $V$ as a function of the shape parameter $m$ alike to that found in the case of homogeneous symmetry breaking in all pendula (compare Figs. 5 and 9), as expected. We found that the $m$ value at which the absolute value of $V$ presents a maximum, $m_{\max}(N)$, decreases monotonously with the number of leaves, while the corresponding absolute value of the maximum average velocity $V_{\max} \equiv V(m = m_{\max}(N))$ does not depend significantly on $N$, indicating again self-organized criticality, as is shown in Fig. 10. In the strong coupling regime again, one systematically obtains $m_{\max}(N) \gtrsim m_{\max}^{unif} \approx 0.989$ for (almost) any value of the SN size and the same remaining parameters as in the complementary case, which is in agreement with the predictions from the criticality scenario discussed above. Indeed, the energy flow now goes on average from the hub to the leaves, increasing the average kinetic energy of the leaves less the larger the

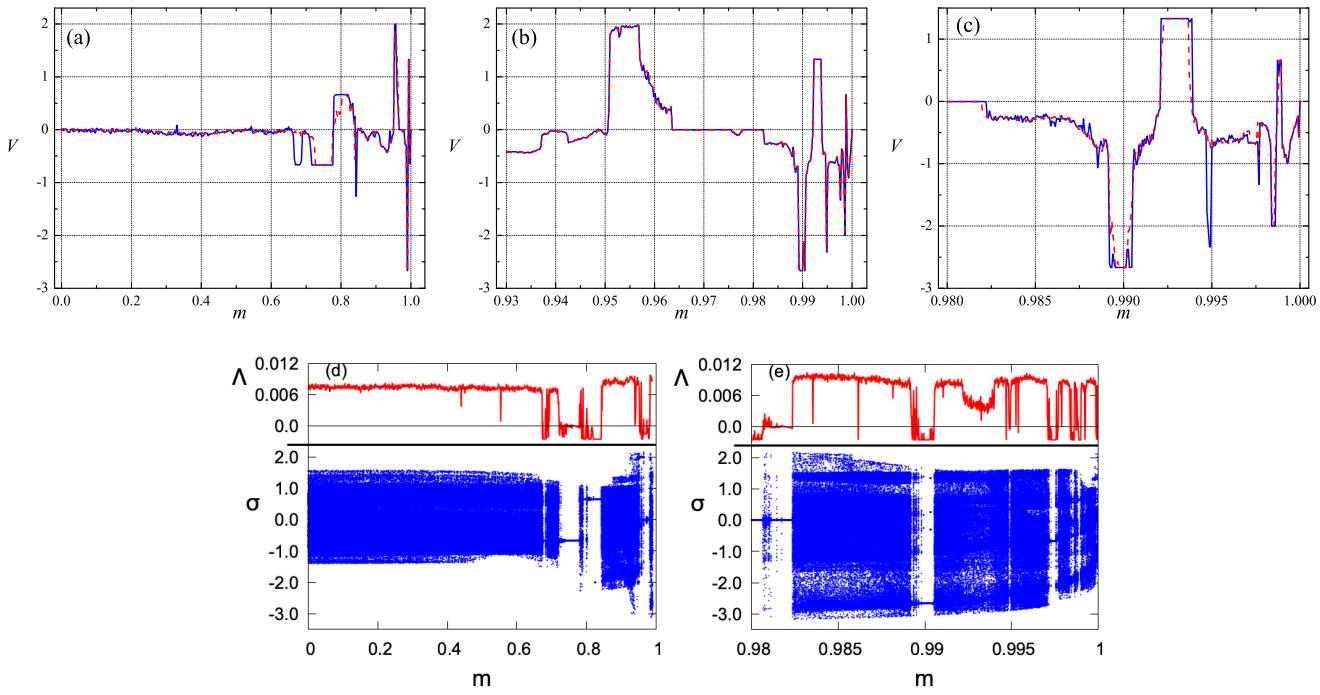


FIG. 5: (a), (b), (c) Average velocity $V$ [cf. Eq. (22)] as a function of the shape parameter $m$ for a homogeneous periodic excitation and two values of the coupling: $\lambda = 4$ (solid line) and $\lambda = 0.01$ (dashed line). Versions (b) and (c) show successive magnifications of version (a) around the maximum of the average velocity at $m = m_{\max}^{unif} \approx 0.989$. (d) Bifurcation diagrams of the average velocity $\sigma$ [cf. Eq. (21)] [blue (black) dots] and maximal LE $\Lambda$ [red (gray) line] as a function of the shape parameter $m$ for a homogeneous periodic excitation and $\lambda = 4$. (e) Magnification of version (d) around the value $m = m_{\max}^{unif} \approx 0.989$. Fixed parameters: $N = M = 10$, $\delta = 0.1$, $\gamma = 4$, $T = 9.43$. The quantities plotted are dimensionless.

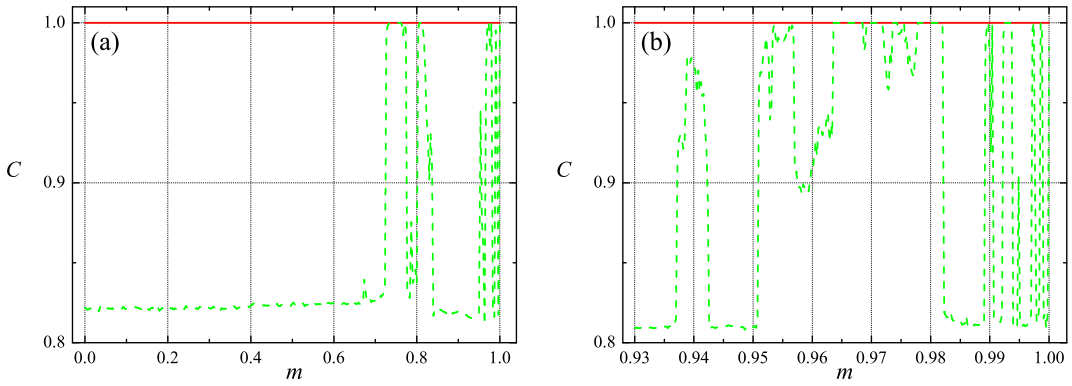


FIG. 6: (a), (b) Average correlation $C$ [cf. Eq. (24)] as a function of the shape parameter $m$ for the same parameters as in Fig. 5. Version (b) shows a magnification of version (a) around $m = m_{\max}^{unif} \approx 0.989$. The quantities plotted are dimensionless.

number of leaves. Since DRT originates now from all the leaves, a greater degree of symmetry breaking is needed to command the motion of the hub than in the case of homogeneous symmetry breaking, and one would expect this symmetry breaking to be closer to that predicted by the RU law $\left(m = m_{\max}^{unif} \approx 0.989\right)$ the larger the number of leaves, in accordance to the degree of symmetry breaking mechanism (see Fig. 10).

Next, we will comment on the structural stability of the present DRT scenario as the coupling constant is decreased from the strong coupling regime to the weak one. Figure 11 shows an illustrative instance of a deliberately chosen unfavorable case for DRT since desynchronization states and amplitude death phenomena appear over a wide range of coupling values (see Fig. 11 middle). One sees, however, the persistence of significant DRT over two narrow ranges of the shape parameter (cf. Figs. 11 top and 11 middle) which correspond to two extrema of the

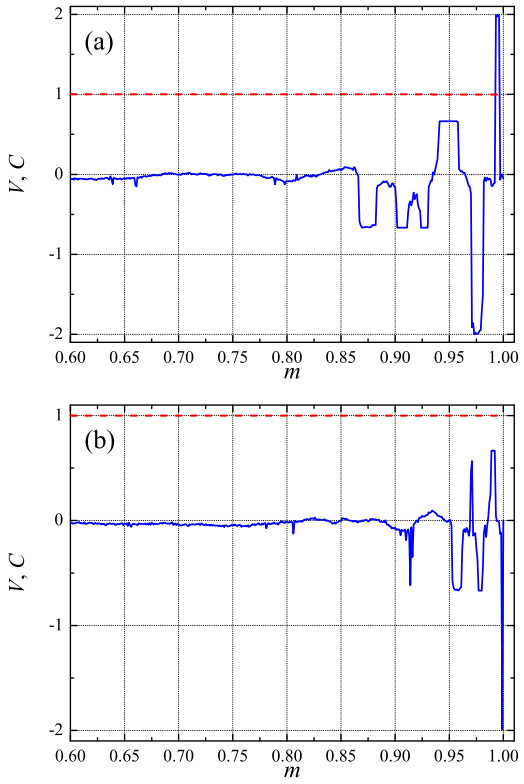


FIG. 7: Average velocity $V$ [cf. Eq. (22)] (solid lines) and average correlation $C$ [cf. Eq. (24)] (dashed lines) as a function of the shape parameter $m$ for starlike networks where symmetry breaking solely occurs in the hub and two values of the network size: (a) $N = 3$, (b) $N = 6$. Fixed parameters: $M = 1$, $\delta = 0.1$, $\gamma = 4$, $T = 9.43$, $\lambda = 8$. The quantities plotted are dimensionless.

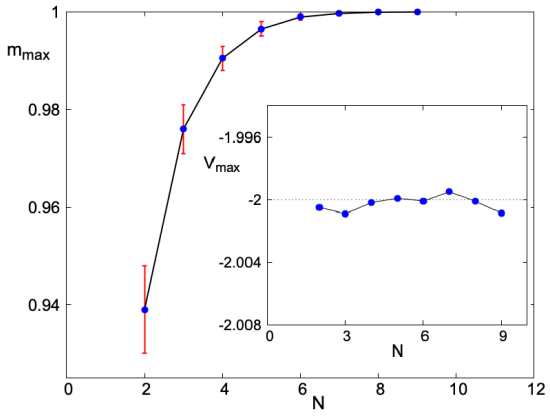


FIG. 8: Shape parameter $m = m_{\max}$ corresponding to extremum average velocity versus network size $N$ for starlike networks where symmetry breaking solely occurs in the hub. The vertical symbols indicate the width of the $m$ range wherein the average velocity remains constant. Inset: Corresponding average velocity $V_{\max} \equiv V\,(m = m_{\max}\,(N))$ versus network size $N$. Fixed parameters: $M = N - 1$, $\delta = 0.1$, $\gamma = 4$, $T = 9.43$, $\lambda = 3.3$. The quantities plotted are dimensionless and the lines are solely plotted to guide the eye.

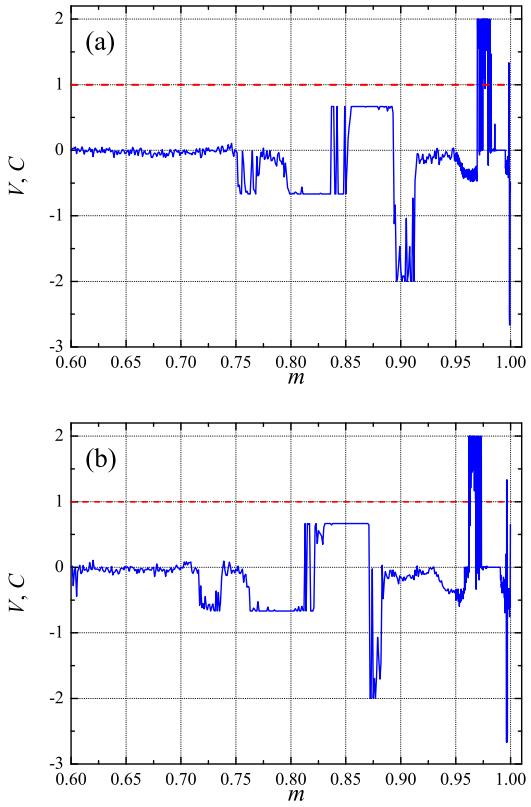


FIG. 9: Average velocity $V$ [cf. Eq. (22)] (solid lines) and average correlation $C$ [cf. Eq. (24)] (dashed lines) as a function of the shape parameter $m$ for starlike networks where symmetry breaking homogeneously occurs in all pendula except in the hub and two values of the network size: (a) $N = 3$, (b) $N = 5$. Fixed parameters: $M = N - 1$, $\delta = 0.1$, $\gamma = 4$, $T = 9.43$, $\lambda = 8$. The quantities plotted are dimensionless.

average velocity and are both centered on values of $m$ that are greater than $m_{\max}^{unif}$, as expected from the above discussion (see Fig.11 bottom).

## IV. CONCLUSIONS AND OUTLOOK

To sum up, the main contribution of the present work is the explanation of the maximum strength of directed ratchet transport in starlike networks of driven damped pendula from a physical self-organized criticality scenario which emerges from a subtle balance between the energy transmitted through the pendula via excitations' impulse and the degree of symmetry breaking. To the best of our knowledge, there is no alternative explanation for the present directed ratchet transport scenario. In this regard, it should be emphasized that previous theoretical approaches based on perturbative methods, such as harmonic mixing (see, e.g., the reviews [49,50] and references therein), which were introduced long ago to quantitatively explain rectification mechanisms, clearly failed to

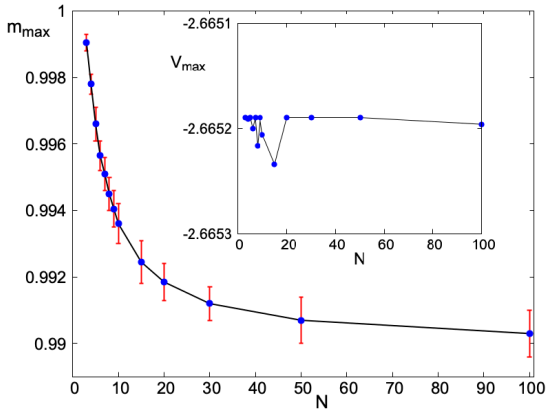


FIG. 10: Shape parameter $m = m_{\max}$ corresponding to extremum average velocity versus network size $N$ for starlike networks where symmetry breaking homogeneously occurs in all pendula except in the hub. The vertical bars indicate the width of the $m$ range wherein the average velocity remains constant. Inset: Corresponding average velocity $V_{\max} \equiv V\,(m = m_{\max}\,(N))$ versus network size $N$. Fixed parameters: $M = N - 1$, $\delta = 0.1$, $\gamma = 4$, $T = 9.43$, $\lambda = 3.3$. The quantities plotted are dimensionless and the lines are solely plotted to guide the eye.

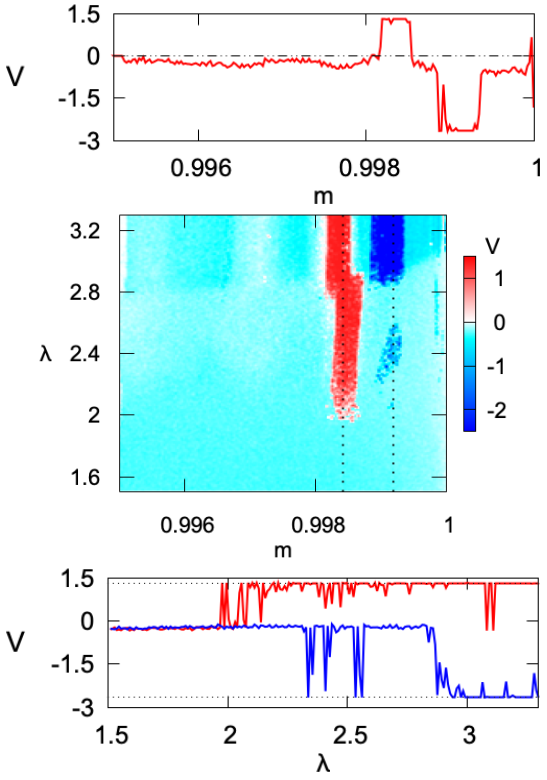


FIG. 11: Top: Average velocity $V$ [cf. Eq. (22)] vs shape parameter $m$ for starlike networks where symmetry breaking homogeneously occurs in all pendula except in the hub and $\lambda = 3.3$. Middle: Averege velocity $V$ versus shape parameter $m$ and period $T$. The vertical dotted lines indicate the values $m = m_1 \equiv 0.998418$ and $m = m_2 \equiv 0.999192$. Bottom: Average velocity $V$ versus coupling $\lambda$ for the values $m = m_1$ (uppermost line) and $m = m_2$. Fixed parameters: $N = 3, M = 2, \delta = 0.1, \gamma = 4, T = 9.43$.

explain both experimental [36] and numerical results [28-31], while the theory of ratchet universality provided satisfactory explanations. Additionally, we have shown that the emergence of chaos mainly depends upon the impulse transmitted by the periodic excitations, thus confirming the chaos scenario found in previous related works [51,52] in which directed ratchet transport was not studied.

Specifically, we have demonstrated the effectiveness and accuracy of the predictions from the ratchet universality law in starlike networks of damped pendula driven by periodic symmetry-breaking-inducing excitations when all pendula are homogeneously driven. In the case of heterogeneous distributions of the periodic driving, in which some pendula are sinusoidally (symmetrically) driven, the ratcheting effect of increasing the breakage of the shift symmetry of periodic excitations acting on the remaining pendula strongly depends upon their number and degree of connectivity as well as the coupling strength. Remarkably, the critical values of the shape parameter for which the strength of directed ratchet transport is maximum in heterogeneous cases can also be explained from a self-organized criticality scenario emerging from a subtle balance between the energy transmitted through the pendula via excitations' impulse and the degree of symmetry breaking. Furthermore, the present directed-ratchet-transport scenario has been shown to be robust against changes in the strength of network connectivity, in the sense that the predictions from the ratchet universality theory hold over wide ranges of values of the coupling constant in which synchronized rotation states dominate the network's dynamics.

Importantly, we expect that an experimental test of the present criticality scenario can be readily achieved in the context of networks of AC-driven Josephson junctions [53,54]. Finally, our results suggest that the present self-organized criticality scenario may be useful at optimally controlling directed ratchet transport in complex networks of the same driven damped pendula, including the ubiquitous case of scale-free networks, since a highly connected pendulum in such a network can be considered as a hub of a locally starlike fragment of the network, while its effectiveness in the cases of one-way coupling and different coupling functions represent exciting next steps for future investigation.

### Acknowledgments

Financial support from the Ministerio de Ciencia, Innovación y Universidades (MICIU, Spain) through Project No. PID2019-108508GB-I00/AEI/10.13039/501100011033 cofinanced by FEDER funds (R.C., A.M.G.-H.) and from the Junta de Ex-

tremadura (JEx, Spain) through Project No. GR24101 cofinanced by FEDER funds (R.C.) is gratefully acknowledged. P.J.M. acknowledges financial support from the Ministerio de Ciencia, Innovación y Universidades (MICIU, Spain) through Project No. PID2020-113582GB-I00/AEI/10.13039/501100011033 cofinanced by FEDER funds and from Departamento de Industria e Innovación del Gobierno de Aragón (FENOL group, Grant No. E36-23R).

[1] Y.-Y. Liu, J.-J. Slotine, and A.-L. Barabási, Controllability of complex networks, Nature **473**, 167 (2011).
[2] T. Nepusz and T. Vicsek, Controlling edge dynamics in complex networks, Nat. Phys. **8**, 568 (2012).
[3] M. Pósfai, Y.-Y. Liu, J.-J. Slotine, and A.-L. Barabási, Effect of correlations on network controllability, Sci. Rep. **3**, 1067 (2013).
[4] S. P. Cornelius, W. L. Kath, and A. E. Motter, Realistic control of network dynamics, Nat. Commun. **4**, 1942 (2013).
[5] G. Menichetti, L. Dall'Asta, and G. Bianconi, Network controllability is determined by the density of low in-degree and out-degree nodes, Phys. Rev. Lett. **113**, 078701 (2014).
[6] J. L. Mateos, Chaotic transport and current reversal in deterministic ratchets, Phys. Rev. Lett. **84**, 258 (2000).
[7] Z. Csahók, F. Family, and T. Vicsek, Transport of elastically coupled particles in an asymmetric periodic potential, Phys. Rev. E **55**, 5179 (1997).
[8] U. E. Vincent, A. Kenfack, A. N. Njah, and O. Akinlade, Bifurcation and chaos in coupled ratchets exhibiting synchronized dynamics, Phys. Rev. E **72**, 056213 (2005).
[9] U. E. Vincent, A. Kenfack, D. V. Senthilkumar, D. Mayer, and J. Kurths, Current reversals and synchronization in coupled ratchets, Phys. Rev. E **82**, 046208 (2010).
[10] P. J. Martínez and R. Chacón, Disorder induced control of discrete soliton ratchets, Phys. Rev. Lett. **100**, 144101 (2008).
[11] Du-Qu Wei, Xiao-Shu Luo, Hong-Bin Chen, and Bo Zhang, Random long-range interaction induced synchronization in coupled networks of inertial ratchets, Chin. Phys. Lett. **28**, 110501 (2011).
[12] Du-Qu Wei, Xian-Hui Mai, Hong-Bin Chen, Xiao-Shu Luo, Bo Zhang, Shang-You Zeng, and Guo-Ning Tang, Transport properties of inertial particles in networks with random long-range interactions, Physica A **394**, 358 (2014).
[13] R. Albert and A.-L. Barabási, Statistical mechanics of complex networks, Rev. Mod. Phys. **74**, 47 (2002).
[14] R. Chacón, *Control of Homoclinic Chaos by Weak Periodic Perturbations* (World Scientific, Singapore, 2005).
[15] A. Pikovsky, M. Rosenblum, and J. Kurths, *Synchronization: A Universal Concept in Nonlinear Science* (Cambridge University Press, Cambridge, 2001).
[16] L. M. Pecora, Synchronization conditions and desynchronization patterns in coupled limit-cycle and chaotic systems, Phys. Rev. E **58**, 347 (1998).
[17] Z. Ma, G. Zhang, Y. Wang, and Z. Liu, Cluster synchronization in star-like complex networks, J. Phys. A: Math. Theor. **41**, 155101 (2008).
[18] A. Bergner, M. Frasca, G. Sciuto, A. Buscarino, E. J. Ngamga, L. Fortuna, and J. Kurths, Remote synchronization in star networks, Phys. Rev. E **85**, 026208 (2012).
[19] P. V. Kuptsov and A. V. Kuptsova, Variety of regimes of starlike networks of Hénon maps, Phys. Rev. E **92**, 042912 (2015).
[20] C. Xu, J. Gao, S. Boccaletti, Z. Zheng, and S. Guan, Synchronization in starlike networks of phase oscillators, Phys. Rev. E **100**, 012212 (2019).
[21] R. Chacón, Optimal control of ratchets without spatial asymmetry, J. Phys. A: Math. Theor. **40**, F413-F419 (2007).
[22] R. Chacón, Criticality-induced universality in ratchets, J. Phys. A: Math. Theor. **43**, 322001 (2010); Corrigendum: Criticality-induced universality in ratchets (2010 J. Phys. A: Math. Theor. 43 322001), *ibid.* **54**, 209501 (2021).
[23] R. Chacón and P. J. Martínez, Exact universal excitation waveform for optimal enhancement of directed ratchet transport, Int. J. Bifurcation Chaos **31**(7), 2150109 (2021).
[24] T. Salger, S. Kling, T. Hecking, C. Geckeler, L. Morales-Molina, and M. Weitz, Directed transport of atoms in a Hamiltonian quantum ratchet, Science **326**, 1241-1243 (2009).
[25] M. Rietmann, R. Carretero-González, and R. Chacón, Controlling directed transport of matter-wave solitons using the ratchet effect, Phys. Rev. A **83**, 053617 (2011).
[26] V. Berardi, J. Lydon, P. G. Kevrekidis, C. Daraio, and R. Carretero-González, Directed ratchet transport in granular chains, Phys. Rev. E **88**, 052202 (2013).
[27] C. E. Creffield and F. Sols, Coherent ratchets in driven Bose-Einstein condensates, Phys. Rev. Lett. **103**, 200601 (2009).
[28] P. J. Martínez and R. Chacón, Ratchet universality in the presence of thermal noise, Phys. Rev. E **87**, 062114 (2013).
[29] P. J. Martínez and R. Chacón, Erratum: Ratchet universality in the presence of thermal noise [Phys. Rev. E **87**, 062114], Phys. Rev. E **88**, 019902(E) (2013).
[30] P. J. Martínez and R. Chacón, Reply to "Comment on 'Ratchet universality in the presence of thermal noise' ", Phys. Rev. E **88**, 066102 (2013).
[31] R. Chacón and P. J. Martínez, Controlling directed ratchet transport of driven overdamped Brownian particles subjected to a vibrating periodic potential: ratchet universality versus harmonic-mixing perturbation theory, Nonlinear Dyn. **104**, 2411 (2021).
[32] J. Xu and X. Luo, Ratchet effects of a Brownian particle with non-Gaussian noise driven by a biharmonic force, Mod. Phys. Lett. B **33**, 1950230 (2019).
[33] L. Lin, L. Yu, W. Lv, and H. Wang, Ratchet motion and current reversal of Brownian motors coupled to birth-death interactions in the crowded environment, Chin. J. Phys. **68**, 808 (2020).
[34] R. Chacón, P. J. Martínez, J. M. Marcos, F. J. Aranda, and J. A. Martínez, Ratchet universality in the bidirec-

tional escape from a symmetric potential well, Phys. Rev. E **103**, 022203 (2021).
[35] P. J. Martínez and R. Chacón, Ratchet universality in coupled oscillators without external bias, Phys. Rev. E **104**, 024224 (2021).
[36] R. Chacón and P. J. Martínez, Directed ratchet transport of cold atoms and fluxons driven by biharmonic fields: a unified view, Phys. Rev. E **104**, 014120 (2021).
[37] P. J. Martínez and R. Chacón, Ratchet universality in the directed motion of spheres by unbiased driving forces in viscous fluids, Nonlinear Dyn. **111**, 12973 (2023).
[38] J. Nath, S. Das, A. Vishwakarma, and A. DasGupta, Direct transport of a particle on a horizontal surface under asymmetric vibrations, Physica D **440**, 133452 (2022).
[39] E. G. Gwinn and R. M. Westervelt, Intermittent chaos and low-frequency noise in the driven damped pendulum, Phys. Rev. Lett. **54**, 1613 (1985).
[40] G. L. Baker and J. A. Blackburne, *The Pendulum: A Case Study in Physics* (Oxford University Press, Oxford, 2005).
[41] P. F. Byrd and M. D. Friedman, *Handbook of Elliptic Integrals for Engineers and Scientists* (Springer-Verlag, Berlin, 1971).
[42] V. K. Melnikov, On the stability of the center for time periodic perturbations, Trans. Moscow Math. Soc. **12**, 1 (1963) [Tr. Mosk. Ova. **12**, 3 (1963)].
[43] J. Guckenheimer and P. Holmes, *Nonlinear Oscillations, Dynamical Systems, and Bifurcations of Vector Fields* (Springer-Verlag, New York, 1983).
[44] A. Pikovsky and A. Politi, *Lyapunov Exponents* (Cambridge University, Cambridge, England, 2016).
[45] S. C. Milne, Infinite families of exact sums of squares formulas, Jacobi elliptic functions, continued fractions, and Schur functions, The Ramanujan Journal **6**, 7-149 (2002).
[46] R. Xiao, L.-W. Kong, Z.-K. Sun, and Y.-C. Lai, Predicting amplitude death with machine learning, Phys. Rev. E **104**, 014205 (2021).
[47] I. S. Gradshteyn and I. M. Ryzhik, *Table of Integrals, Series, and Products* (Academic Press, San Diego, 1980).
[48] R. Chacón, F. Palmero, and J. Cuevas-Maraver, Impulse-induced localized control of chaos in starlike networks, Phys. Rev. E **93**, 062210 (2016).
[49] P. Hänggi and F. Marchesoni, Artificial Brownian motors: Controlling transport on the nanoscale, Rev. Mod. Phys. 81, 387 (2009).
[50] S. Denisov, S. Flach, and P. Hänggi, Tunable transport with broken space-time symmetries, Phys. Rep. 538, 77 (2014).
[51] R. Chacón, F. Palmero, and J. Cuevas-Maraver, Impulse-induced localized control of chaos in starlike networks, Phys. Rev. E **93**, 062210 (2016).
[52] R. Chacón, A. Martínez García-Hoz, and F. Palmero, Amplitude modulation control of spatiotemporal chaos in starlike networks of damped-driven pendula, Physica D **457**, 133950 (2024).
[53] A. Barone and G. Paterno, *Physics and Applications of the Josephson Effect* (John Wiley & Sons, New York, 1982).
[54] M. Lorenzo et al., On Bose-Einstein condensation in Josephson junctions star graph arrays, Phys. Lett. A 378, 655 (2014).